The nature of bilateral supernova remnants

B. M. Gaensler[1,2]

February 1, 2008

This paper has been accepted to *The Astrophysical Journal*.

ABSTRACT

We present high-resolution radio images at 1.4 GHz of two Galactic supernova remnants (SNRs), G003.8–00.3 (formerly G003.7–00.2) and G350.0–02.0 (formerly G350.0-01.8). Although the two objects are very different in appearance, in both cases the radio emission shows a clear bilateral (or "barrel") morphology for which the axis is parallel to the Galactic Plane.

The majority of Galactic SNRs have now been observed at high resolution, and one can define a clear bilateral subset of the population. We consider a sample of 17 such SNRs, and find a highly significant tendency for the bilateral axes of these SNRs to be aligned with the Galactic Plane. We interpret this as indicating that "extrinsic" effects dominate the morphology of such remnants. Specifically, we argue that the Galactic magnetic field causes these SNRs to appear bilateral, either directly, in the form of magnetic field compression and/or quasi-perpendicular acceleration of electrons in the supernova shock, or more likely indirectly, by pre-processing the interstellar medium to produce density stratifications extended along the Plane.

Subject headings: Galaxy: structure — ISM: magnetic fields, structure — shock waves — supernova remnants: individual (G003.8–00.3, G350.0–02.0)

[1]Australia Telescope National Facility, CSIRO, PO Box 76, Epping, NSW 2121, Australia

[2]Astrophysics Department, School of Physics A29, University of Sydney, NSW 2006, Australia; b.gaensler@physics.usyd.edu.au

1. Introduction

High resolution observations of radio supernova remnants (SNRs) have revealed exceedingly complex structures. The appearance of a SNR can tell us much about the supernova (SN) explosion itself, the nature of any central compact object, the circumstellar medium (CSM) of the progenitor, the surrounding interstellar medium (ISM), and the properties of the ambient magnetic field. Indeed the difficulty in interpreting SNR morphologies has always been in disentangling the competing effects and in determining which ones dominate during the different evolutionary stages.

Perhaps the longest running debate concerning SNR morphologies has been over the classification referred to as bilateral, bipolar, axially symmetric, or "barrel" SNRs. These remnants are characterised by a clear axis of symmetry, low levels of emission along this axis, and two bright limbs on either side (e.g. Gardner & Milne 1965; Whiteoak & Gardner 1968; Roger & Costain 1976; Kesteven & Caswell 1987, hereafter KC87; Roger *et al.* 1988; Caswell *et al.* 1992). It is generally accepted that bilateral SNRs represent an underlying cylindrical symmetry, the emitting regions corresponding to the curved walls of the cylinder (KC87). A bilateral appearance is then produced when the "barrel" axis is approximately in the plane of the sky, the two bright flanks running parallel to this axis.

Many mechanisms for generating a bilateral appearance have been suggested (see Bisnovatyi-Kogan & Silich 1995 for a review). However it is not clear which of these models, if any, actually apply. Indeed, given the diversity in the environments and ages of Galactic SNRs, several of the mechanisms proposed may be valid. We emphasise that observations demonstrate that many SNRs are not bilateral. To some extent, this can be accounted for by viewing angle (see KC87 and Section 6.4 below), but it is important to keep in mind that whatever mechanism is invoked, the morphology may be dominated by small scale effects such as the inhomogeneity of the local environment.

We now briefly outline previously proposed explanations for bilateral SNRs. Explanations can be divided up into two categories: "extrinsic", relating to the ambient ISM and magnetic field, and "intrinsic", relating to the progenitor, its CSM, the SN explosion itself, and any compact stellar remnant.

1.1. Extrinsic explanations

The simplest model to explain a bilateral appearance is that it is the result of the density structure of the surrounding ISM. Simulations show that when a remnant expands inside an elongated, or tube-like, cavity, it quickly takes the shape of that cavity, and a

bilateral appearance can be produced (Bisnovatyi-Kogan, Lozinskaya, & Silich 1990).

It has long been realised that the geometry of the ambient magnetic field can also affect the appearance of a SNR. We collectively refer to models relying on the ambient field as "magnetic". In a uniform magnetic field, the shock front produced by an expanding SNR will preferentially compresses the field where the shock normal is perpendicular to the field lines. Thus, in a well-ordered ambient field with a significant component in the plane of the sky, enhanced emission along two limbs is generated, producing a bilateral appearance (van der Laan 1962; Whiteoak & Gardner 1968).

Argument is divided as to whether this mechanism can produce the observed ratio of maximum to minimum intensity around the circumference of SNRs which are in the adiabatic phase of evolution (Fulbright & Reynolds 1990, hereafter FR90; Ratkiewicz, Axford, & McKenzie 1994). Thus, an extension of this model has been proposed, in which the efficiency of particle acceleration by the SN shock depends on the angle between the shock normal and the orientation of the ambient magnetic field (Jokipii 1987; Roger *et al.* 1988; FR90). FR90 argue that the bilateral appearance in the adiabatic phase can best be explained by "quasi-perpendicular" acceleration, in which acceleration is most efficient (and synchrotron emission strongest) where the shock normal and the field are at right angles. "Quasi-parallel" models (where the shock normal and the field are aligned) can also produce a bilateral appearance at some orientations, but at other orientations produce morphologies which are never observed (FR90, but see Zhang, Wang, & Chen 1996).

1.2. Intrinsic explanations

There are a number of symmetry axes associated with the progenitor system and the explosion. Several mechanisms have been suggested by which these symmetries can produce a bilateral appearance. Models include a toroidal distribution of ejecta (Bodenheimer & Woosley 1983; KC87), the effect of a high velocity progenitor (Różyczka *et al.* 1993; Brighenti & D'Ercole 1994), the distribution of mass loss and magnetic field in the CSM produced by the progenitor (Manchester 1987; Igumenshchev, Tutokov, & Shustov 1992; Storey *et al.* 1992; Zhang, Wang, & Chen 1996), and the influence of outflows from a central compact object (Manchester & Durdin 1983; Willingale *et al.* 1996).

1.3. A statistical approach

Understanding the morphology of an individual SNR can be difficult, often requiring a concerted multi-wavelength campaign. Only a few bilateral SNRs can be considered to be well-studied (most notably G296.5+10.0 and G327.6+14.6) and even these objects provoke controversy (e.g. compare Roger *et al.* 1988 with Storey *et al.* 1992). An alternative approach is to consider the common properties of bilateral SNRs on a statistical basis.

There is reasonable evidence that at least for low latitudes, the Galactic magnetic field is well-ordered and generally runs parallel to the Galactic Plane when projected onto the sky (Mathewson & Ford 1970; Manchester 1974; Ellis & Axon 1978; Sofue & Fujimoto 1983; Rand & Kulkarni 1989; Reid & Silverstein 1990; see also reviews by Sofue, Fujimoto, & Wielebinski 1986 and Beck *et al.* 1996). If a bilateral appearance is caused by a magnetic model, one might expect the structure of the Galactic magnetic field to manifest itself as a statistical alignment of the symmetry axes of bilateral SNRs with the Galactic Plane (Shaver 1969).

Given that such a result would be reasonably conclusive, several researchers have attempted to determine whether such an alignment exists. By creating an average circumferential profile from SNRs for which appropriate data was available at the time, Shaver (1969) found that SNRs appeared to have minima in their emission where the shell is intersected by a line of constant Galactic latitude, and argued that this was evidence for magnetic models. However, the statistical significance of the result was low, and the limited sample available was from observations of poor resolution and sensitivity.

In more recent years, the statistics of SNR samples have steadily improved, and other researchers have carried out various analyses investigating alignment between the axes of SNRs (defined in various ways) and the Galactic Plane (Shaver 1982; Manchester 1987; Leckband, Spangler, & Cairns 1989; Whiteoak & Green 1996, hereafter WG96). In all cases, no alignment was found, leaving the authors to conclude that either the magnetic field is not well-aligned with the Plane at such scales, or that the magnetic model is not valid.

However, some of these studies implicitly assume that *all* SNRs have a bilateral symmetry, and then assign an axis to every remnant in their sample. Others restrict their sample to SNRs with a symmetry axis, but include remnants where this symmetry is not necessarily bilateral. If only a small subset of remnants are truly bilateral, then these analyses will never show any alignment because any real effect will be swamped by the large number of randomly oriented axes corresponding to non-bilateral SNRs. In addition, the low resolution of many of the images available at the time caused a poor determination of the axis of symmetry.

There are now over 200 SNRs known in the Galaxy (Green 1996), and an increasing number of objects have been observed at high resolution. For almost the entire Galactic population, observations are now of sufficient quality that one can determine which SNRs have a clear bilateral appearance (defined in some manner), and restrict analysis to this sample.

In Section 2, we describe high-resolution 1.4 GHz observations and analysis procedures for two Southern SNRs, G003.8–00.3 (formerly G003.7–00.2) and G350.0–02.0 (formerly G350.0–01.8). We present images of these remnants in Section 3, and argue that these SNRs are members of the bilateral class with their axes aligned along the Galactic Plane. The properties of these two SNRs are then briefly discussed in Section 4. In Section 5, we consider the Galactic population of bilateral SNRs, and demonstrate a clear tendency for the bilateral axis to align with the Plane. It is argued in Section 6 that the magnetic model can explain this alignment, but that there are difficulties accounting for the detailed morphologies of bilateral SNRs. An alternative model is proposed, in which the ISM is pre-processed by the ambient magnetic field to form structures running parallel to the Galactic Plane. SNRs then interact with this material, producing a bilateral appearance with the observed alignment.

2. Observations and data reduction

Interferometric observations were made with the Very Large Array (VLA) of the National Radio Astronomy Observatory[3], an aperture synthesis telescope consisting of 27 antennae in a "Y"-shaped array, located near Socorro, New Mexico (Napier, Thompson, & Ekers 1983). The dates and lengths of the observations are given in Table 1. Two bands were observed simultaneously, with centre frequencies of 1.385 GHz and 1.465 GHz, bandwidths of 50 MHz, in all four Stokes parameters. Because of its large angular extent, SNR G350.0–02.0 was observed in a mosaic of four pointings (see Table 3), with a cycle time of 24 minutes. Amplitudes were calibrated by assuming flux densities at 1.385 and 1.465 GHz respectively of 14.94 and 14.55 Jy for J1331+305 (3C286) and 16.32 and 15.62 Jy for J0137+331 (3C48), where 1 Jy = 10^{-26} W m^{-2} Hz^{-1}. Phases were calibrated using the source J1751–253.

The VLA data were edited and then calibrated in AIPS using standard techniques (Greisen 1996). The visibility data were then transferred to the Miriad package (Sault,

[3]The National Radio Astronomy Observatory is a facility of the National Science Foundation operated under cooperative agreement by Associated Universities, Inc.

Teuben, & Wright 1995), and total intensity images formed using uniform weighting and a cell size of $4''$. For the mosaiced observations of G350.0–02.0, a joint image was formed from all four pointings (Cornwell, Holdaway, & Uson 1993; Sault, Staveley-Smith, & Brouw 1996), which was then corrected for the mean primary beam response of the VLA antennae.

The smallest projected spacing between antennae for the observations in Table 1 is 0.12 kλ , which corresponds to an angular scale of $\sim 30'$. Thus the VLA observations are not sensitive to emission on scales larger than this. These short spacings were obtained by making single-dish observations (in total intensity only) of both SNRs using the Parkes 64m radio telescope[4]. Amplitudes were calibrated using the source PKS B1934–638, assuming a flux density of 14.90 Jy. Except where noted in Table 2, observational techniques were the same as used in the 2.4 GHz survey of Duncan *et al.* (1995). Scans were made in both l and b, of regions surrounding both SNRs, at a scan rate of 6° min^{-1}. The Parkes observations were reduced in the manner described by Duncan *et al.* (1995), and the resultant images regridded and reprojected to match the higher resolution data.

Data from the two telescopes were then combined by adding together the dirty images from each instrument. The flux density scale of the single dish data was preserved by weighting them by the inverse ratio of the beam areas (Ye, Turtle, & Kennicutt Jr. 1991; Stewart *et al.* 1993). Point spread functions were produced similarly, and the images then deconvolved using the maximum entropy algorithm (Gull & Daniell 1978). For G350.0–02.0, all pointings were deconvolved simultaneously using the Miriad task MOSMEM (Sault, Staveley-Smith, & Brouw 1996). The resulting models were then smoothed using a Gaussian restoring beam to produce the final images.

Because of the proximity of G003.8–00.3 to both the Galactic Plane and the Galactic Centre, single-dish observations of this source are dominated by diffuse emission from confusing sources and the Galactic background. The composite image has flux filling the entire field of view, and it is thus not possible to successfully deconvolve it. The image of G003.7–00.2 as presented in Section 3 therefore does not include the Parkes measurements. Since the angular extent of this SNR is significantly smaller than the largest spatial scale sampled by the VLA, we still expect to recover almost all of the flux density from this object.

Images of linearly polarized emission were made from the interferometric data in Stokes Q, U and V. (Although no real emission is expected in circular polarization, the V image provides a useful check of quality.) The Q and U images were then deconvolved using the

[4]The Parkes radio telescope forms part of the Australia Telescope, which is funded by the Commonwealth of Australia for operation as a National Facility managed by CSIRO.

CLEAN algorithm (Clark 1980), and a linear polarization image, L, produced which was then corrected for non-Gaussian noise statistics (Killeen, Bicknell, & Ekers 1986) using the Miriad task IMPOL.

3. Results

Total intensity images of G003.8–00.3 and G350.0–02.0 are shown in Figures 1 and 2 respectively. These images are of higher resolution, and in the latter case, of greater extent than in previous images. We are thus able to derive improved positions for the centres of these two SNRs, resulting in a change of name for both remnants.

Because the VLA is non-coplanar, the approximation of a flat sky used in standard synthesis imaging is invalid at large distances from the phase centre (Perley 1989). As a result, some point sources in Figure 2 have a triangular appearance.

Information about each image and its derived parameters are provided in Table 3. Flux densities and their uncertainties were determined by integrating within multiple polygons enclosing the emission from each SNR. The RMS noise in each image was measured by similarly integrating over a source-free region. In the case of G003.8–00.3, the given centre and diameter are those of a circle best fitting the outer perimeter of the emission. G350.0–02.0 is clearly non-circular, and so the centre is defined as that point equidistant from the boundaries of the SNR both along and at right angles to the bilateral axis. The diameter given is the maximum extent in these two directions.

3.1. G003.8–00.3

SNR G003.8–00.3 (then G003.7–00.2) was discovered in the Galactic Centre Survey carried out with the Molonglo Observatory Synthesis Telescope (MOST) at 0.843 GHz (Gray 1994) and was classified as a SNR on the basis of its morphology. Using flux densities from Gray (1994) and from Table 3, we obtain a spectral index for G003.8–00.3 of $\alpha = -0.65 \pm 0.05$ ($S_\nu \propto \nu^\alpha$), confirming the non-thermal nature of this source.

The image of G003.8–00.3 (Figure 1) shows it to be a classic bilateral remnant, with a clear axis of symmetry defined by the two bright limbs, and a low level of emission along this axis (cf. KC87). The emitting regions appear to be composed of multiple filaments extended along the symmetry axis: on the north-west rim of the SNR, these filaments take the form of roughly parallel arcs, while in the south-east they overlap each other. The original 0.843 GHz image of this remnant seemed to contain multiple overlapping rings

(Gray 1994). However this appearance is most probably due to the alignment of various filaments when seen with the lower resolution of the MOST — no such features are evident in our image.

ψ is defined to be the acute angle between the symmetry axis of the SNR and the Galactic Plane. We fit the symmetry axis by eye, and estimate the uncertainty by fitting a set of possible axes to the remnant. This gives a value $\psi = 6^\circ \pm 2^\circ$, indicating close alignment between the symmetry axis and the Plane. More involved methods for determining ψ (e.g. Storey *et al.* 1992) were also implemented, giving similar results. For the accuracy required for ψ in this work, the more rigorous determinations are not warranted. Furthermore, for several sources considered in Section 5.3, images were not available in electronic form.

Weak linearly polarized emission fills the entire image, and it is not possible to determine how much emission is specifically associated with the remnant. We put an upper limit of 0.05 Jy on polarized emission from G003.8–00.3, corresponding to a fractional polarization of <3%.

3.2. G350.0–02.0

SNR G350.0–02.0 (then G350.0–01.8) was first identified from a 408 MHz survey of the Galactic Plane carried out with the Molonglo Cross (Green 1972). At the comparatively low resolution and sensitivity of the time, only the bright north-western arc was clearly delineated. For the next 20 years, this remnant received little attention: Clark *et al.* (1975) suggested it was "part of an old large SNR", Caswell (1977) noted it as an example of a SNR which was brighter towards the Galactic Plane, while KC87 described it as "difficult to classify". More recent observations at 0.843 GHz (MOST; Burn & Bush 1994) and at 2.4 GHz (Parkes 64m; Duncan *et al.* 1995) have demonstrated that this SNR is of far greater extent than previously realised. Higher resolution VLA observations are shown in Figure 2.

Using a 2.4 GHz flux density of 18 ± 1 Jy (obtained from the single-dish measurements of Duncan *et al.* 1995), and the 1.4 GHz value given in Table 3, we derive a spectral index for G350.0–02.0 of $\alpha = -0.4 \pm 0.1$. Note that the flux density values quoted for this SNR by Clark *et al.* (1975) correspond only to the bright north-west component.

The image of this SNR in Figure 2 shows a far more complicated morphology than previously thought. It may even correspond to multiple remnants, a possibility discussed below in Section 4.2. The brightest region of G350.0–02.0 (corresponding to the previously identified source G350.0–01.8, and labelled as A in Figure 2) consists of several overlapping filaments, with the suggestion of complex, unresolved, structure. This region, which extends

over $\sim 40'$, forms a roughly circular arc with radius of curvature $\sim 55'$. In the remnant's interior is region B, separated from region A by a zone of diffuse emission of width $\sim 8'$. Region B consists of a series of wisps, considerably fainter than the emission in region A, but with a similar orientation and curvature. A third region, C, is separated from region B by another zone of diffuse emission of width $\sim 6'$. Region C consists of still more overlapping filaments, of opposite curvature to the rest of the SNR, which complete a distorted shell of emission. The outer rim of region C forms a circular arc of radius $\sim 14'$, considerably different from the radius of curvature for region A.

Although G350.0–02.0 is clearly very different to G003.8–00.3, it also has a bilateral appearance. The circumference of the remnant is bounded on two sides by regions of significant emission (namely A and C), and at perpendicular position angles the emission is considerably weaker. As for G003.8–00.3, a bilateral axis can be defined. This axis is shown in Figure 2, drawn perpendicular to a line joining the centres of curvature of regions A and C. For this axis, $\psi = 5^\circ \pm 2^\circ$, again a high degree of alignment with the Plane.

Clumps of linear polarization are detected throughout the interior of G350.0–02.0. The total polarized intensity is 0.8 Jy, implying a fractional intensity of 3.6%.

4. Discussion

Because of the lack of information at other wavelengths and the proximity of both remnants to $l = 0^\circ$, the methods typically used to estimate distances to SNRs cannot be applied (see Green 1984). The $\Sigma - D$ relation (e.g. Caswell & Lerche 1979; Huang & Thaddeus 1985) has in the past been used to estimate distances to SNRs, but the uncertainties are large (Green 1984; Berkhuijsen 1986). Thus we conclude that the age of and distance to these SNRs remains unknown at the present time.

4.1. G003.8–00.3

FR90 have quantified the contrast between the brightest and faintest regions of a bilateral SNR by using an "azimuthal intensity ratio", A. This is defined as the ratio between the peak of emission around the SNR shell, and the minimum value around the shell at the radius corresponding to this peak. The filamentary nature of this SNR makes it difficult to compute A in this manner, but we have made a commensurate calculation as follows. The shell of emission from the SNR lies within an annulus of inner radius $4\farcm2$ and outer radius $6\farcm7$, centred on the coordinates for G003.8–00.3 as listed in Table 3. We have

divided this annulus into 360 azimuthal bins, and computed the average flux density in each bin. A peak of approximately 1.1 mJy beam^{-1} occurs at position angles (measured north through east) of 100° and 260°. The minimum level of emission occurs at PA $\approx 40°$, where no emission can be detected above the 3σ noise level. This corresponds to an intensity ratio of $A > 6$, at a resolution of $\sim$70 beams per diameter. For a remnant in the adiabatic phase, this is consistent with magnetic models for a bilateral appearance, but does not distinguish between field compression alone and quasi-perpendicular acceleration (FR90).

4.2. G350.0–02.0

One interpretation for the three spatially and morphologically distinct regions of emission in G350.0–02.0 is that they are two or three separate SNRs, as has been postulated in objects such as G053.6-02.2 (3C400.2; Dubner *et al.* 1994) and 0547–697 (DEM L 316; Williams *et al.* 1997). Certainly regions B and C are of similar surface brightness, which could be interpreted as a complete shell, separate from region A.

If we consider a region on the sky defined by $330° = -30° \leq l \leq 30°$, $1.5° \leq |b| \leq 3°$ (i.e. longitudes and latitudes representative of G350.0–02.0), we find nine SNRs in the catalogue of Green (1996). Given this sky density, the probability of finding two randomly distributed remnants less than $30'$ apart (as required here) is 14%. However, this is probably a lower limit, since the small number of SNRs detected in this region may be due to the incomplete sky coverage of existing surveys. Also, SNRs are not necessarily randomly distributed, but at least for those formed from massive stars probably represent the clustering of their progenitors. Thus there is no convincing statistical argument that G350.0–02.0 is a single SNR.

Nevertheless, the centres of curvature for all three regions lie in a straight line, which bisects the three arcs of emission. The fact that regions A and C are of opposite concavity also suggests that all the emission represents common expansion from a single event. Diffuse emission from the SNR (contributed primarily by the single dish observations) delineates a single plateau of emission bounded by regions A and C. We therefore consider the most likely interpretation to be that the emission in this region is from a single object.

It is possible that the non-circular appearance could be due to the influence of a pulsar or other compact object. An analogy could be drawn with SNR G005.4–01.2, which has a bright, flattened ridge of emission along one side (Caswell *et al.* 1987; Frail, Kassim, & Weiler 1994), resembling region A of G350.0–02.0. It has been proposed that the distorted morphology of this SNR is a result of the associated pulsar PSR B1757–24 overtaking the

expanding parent shell (Frail & Kulkarni 1991). While a flat-spectrum region extending from the pulsar back towards the radio shell supports such a model for SNR G005.4–1.2 (Frail & Kulkarni 1991; Frail, Kassim, & Weiler 1994), no similar component is observed in G350.0–02.0, nor has any pulsar been detected (Manchester, D'Amico, & Tuohy 1985; Kaspi *et al.* 1996). Thus we consider an interaction with a compact object an unlikely explanation for the observed morphology. Given that any associated pulsar should be located near the SNR's presumed centre of expansion (Gaensler & Johnston 1995), the area bounded by regions B and C might be a more fruitful target for future pulsar searches.

A 1.4 GHz image of SNR G166.0+04.3 (VRO 42.05.01; Landecker *et al.* 1982 ; Pineault, Landecker, & Routledge 1987) is shown in Figure 3, revealing a striking resemblance between this SNR and G350.0–02.0. G166.0+04.3 is also composed of three separate regions, whose relative shape, size and orientation are similar to those in G350.0–02.0. Both SNRs are bounded on one side by a bright arc with a large radius of curvature which trails into the noise (region A), contain a fainter strip of emission parallel to A and separated from it (region B), and a series of filaments with a distinctly smaller radius of curvature and of opposite concavity to the rest of the emission, completing the outline of a shell (region C). Both SNRs are similarly aligned to the Galactic Plane: when an axis of symmetry is defined for G166.0+4.3, one finds that $\psi = 2^\circ \pm 2^\circ$.

There are notable differences between the SNRs, however. Firstly, in G350.0–02.0, regions B and C are of similar brightness but are much fainter than A, while in G166.0+04.3, the region corresponding to C (the "shell" of Landecker *et al.* 1982) is of comparable brightness to that corresponding to region A (the "wing"). Secondly, the central region of G166.0+04.3 consists of linear features, while region B appears to be curved. Finally, while in G350.0–02.0 regions B and C are separated by a region of faint emission, the analogues of these two regions in G166.0+04.3 actually overlap.

Pineault *et al.* (1987) explain the morphology of G166.0+04.3 in terms of the interaction of an expanding remnant with a slab of pre-existing low density material. The SN explosion is believed to have occurred at or near the centre of curvature of the "shell" component, which represents the expansion of that part of the SN shock into a uniform medium. The faint linear features in the remnant's centre mark the re-energising of the slab's surface as a result of the shock breaking out into it, and the "wing" component represents the shock once again encountering dense material on the other side.

The similarity between the two remnants suggests a similar explanation for them as well. In this model, region C of G350.0–02.0 is the unperturbed component of the original SNR, which evolves independently of those parts of the remnant which encounter a more complicated structure (Falle & Garlick 1982; Tenorio-Tagle, Bodenheimer, & Yorke 1985).

Indeed, region C resembles SNR G119.5+10.2 (CTA 1; Pineault *et al.* 1993), a partial shell for which there is evidence that a breakout has occurred but for which the remainder of the SN shock is not visible. Region B of G350.0–02.0 represents the boundary of a low density slab. That it is concave and not linear and does not overlap with region C, suggests that the details of the 3D geometry differ from that in the case of G166.0+04.3. Region A is that component of the shock which has traversed the slab and continues to propagate beyond it.

5. The Galactic population of bilateral SNRs

5.1. Selection criteria

Although previous studies have argued that no alignment exists between the axes of bilateral SNRs and the Galactic Plane, it is interesting that G003.8–00.3, G350.0–02.0 and G166.0+04.3 should all have such low values of ψ. This similarity prompted an examination of other bilateral SNRs.

We have therefore reviewed the Galactic SNR catalogue of Green (1996), which currently contains 215 remnants. The criteria for a SNR to be classed as bilateral are as follows:

- It must be of the shell or composite class.
- The highest resolution image available must have a minimum of 10 beams across its diameter.
- The SNR must have clear minima in emission separated by position angles of $180^\circ \pm 30^\circ$ relative to the assumed centre of the SNR. The presence of opposed minima is the main criterion for classification, as it is these minima which define the bilateral axis.
- The SNR must have well-defined maxima, similarly opposed, and at approximately perpendicular position angles to the minima.
- A clear bilateral axis should be identifiable, passing through the two minima and through the centre of the SNR. Objects with a large uncertainty ($\gtrsim 20^\circ$) in the position angle of the axis are excluded — this requirement is critical in defining the objects in the sample.

We do not quantify the azimuthal intensity ratio, A, of FR90 as a threshold. Such a measurement is both difficult and misleading, because of the various presentations of

images in the literature, and of the differing nature of the observations involved. As FR90 have pointed out, the value of A depends strongly on the resolution of an image, so that the appearance of bilaterality will increase with resolution. Also, the lack of large-scale emission present in some interferometric images can cause a further over-estimation of this parameter. Thus using this ratio as a threshold will not result in a consistent criterion.

5.2. Non-bilateral SNRs

There are 198 SNRs in Green's (1996) SNR catalogue which do not meet our criteria. This is in strong contrast to KC87, who found that 63% of all SNRs had some element of "barrel" structure. This primarily reflects the strictness of our criteria. For example, consider G315.4–02.3 (RCW 86; Figure 4) and G332.4–00.4 (RCW 103; Figure 5), both of which are described by KC87 as "well developed barrels". The former has no opposed maxima or minima. The latter is a marginal case (Dickel *et al.* 1996 describe it is an "incipient barrel"), but lacks the distinctive minima and symmetry properties of the best examples of the class.

Improved observations over the last ten years have allowed a more precise classification of many remnants. For the MOST, substantial improvements to both hardware (Amy & Large 1990, 1992) and data reduction techniques (Cram & Ye 1995) since the observations of KC87 were made have significantly reduced the effect of artifacts, increased the sensitivity, and generally improved image quality.

5.3. Bilateral SNRs

There remain 17 remnants in the catalogue which can be classed as clearly bilateral from our criteria. A list of these bilateral SNRs is given in Table 4. For each remnant a bilateral axis is defined by eye, as for the SNRs in Section 3. This axis passes through the two minima, corresponding closely to an axis of mirror symmetry. Some examples of SNRs which we have classed as bilateral are shown in Figures 6 through 11, with the bilateral axis of each remnant shown. In each case, we have measured the acute angle, ψ, between this axis and the Galactic Plane. Values of ψ for each SNR are shown in Table 4.

The reader is encouraged to examine these (and other) SNRs in order to verify that the classifications made are reasonable. We should emphasise that if there is any doubt, a SNR is *excluded* from our class. If a preferential alignment exists, it will remain apparent if some bilateral SNRs are excluded from the sample (provided that the statistics are still

meaningful), but will be masked if too many remnants which do not satisfy the criteria are included.

5.4. Orientation with respect to the Galactic Plane

A histogram of the distribution in ψ from Table 4 is shown in Figure 12. This distribution has a median of $\psi_m = 12^{\circ}{}^{+3^{\circ}}_{-2^{\circ}}$, where the uncertainty corresponds to the maximum shift in median should two objects be discarded from the sample. This result suggests an alignment of bilateral SNRs with the Galactic Plane: the probability of this distribution occurring by chance is now discussed.

Assume cylindrical symmetry for bilateral SNRs, and represent the three-dimensional axis of such a remnant by a vector in Cartesian space, with spherical coordinates θ, ϕ as shown in Figure 13. The observer views the system along the r axis, and the l and b axes represent increasing Galactic longitude and latitude respectively in the plane of the sky. Note that the observed axis is a projection onto the $l - b$ plane of the true axis, and that a remnant will only have a bilateral appearance provided that $\theta > \theta_c$, where θ_c depends on the details of the geometry (KC87). We only consider values in the range $|\phi| \leq 90^{\circ}$, since the other hemisphere is equivalent. Randomly oriented vectors will have a uniform distribution in ϕ and hence in ψ. Thus all values of ψ are equally likely, independent of θ_c.

Using the binomial theorem, we can calculate that the probability of a randomly oriented sample having the observed median is $0.7^{+4.7}_{-0.1} \times 10^{-3}$. We argue in Section 6.3 that G296.5+10.0 and G327.6+14.6 may be distinct from the other objects in Table 4, as a consequence of their large distance from the Plane. These two remnants have the highest values of ψ, and if they are excluded from the sample, the probability is even more tightly constrained.

This calculation shows that the probability of the distribution being randomly oriented is low. *We therefore consider our data to demonstrate strong evidence that bilateral SNRs align with the Galactic Plane.*

Given that no correlation between the Galactic Plane and the rotational axes of SNR progenitors has been observed (Slettebak 1949; Huang & Struve 1954), intrinsic models for the bilateral appearance (as listed in Section 1.2) are not consistent with the observed distribution of ψ. These models are probably better suited to explain the appearance of other classes of remnant morphology. For example, a toroidal explosion may be appropriate for G292.0+01.8 (Tuohy, Clark, & Burton 1982), a high velocity progenitor could describe G357.7-00.1 (Shaver *et al.* 1985; Becker & Helfand 1985), outflows from a central source are

appropriate for G039.7-02.0 (W50 and SS433; Elston & Baum 1987), while the properties of the CSM perhaps only cause a bilateral appearance at an early age, such as is observed in the radio remnant of SN 1987A (Gaensler *et al.* 1997).

6. Models for bilateral SNRs

6.1. A magnetic model

As discussed in Section 1.3, an alignment of bilateral SNRs can be interpreted as evidence for magnetic models (Shaver 1969; Manchester 1987). In order for such mechanisms to be effective, the surrounding magnetic field must be well-ordered and the ISM into which the SNR is expanding must be reasonably homogeneous. The small number of bilateral remnants may indicate that this condition rarely occurs, as will be discussed further below.

There is some support for the magnetic model from polarization measurements. Specifically, in the field compression scenario (Whiteoak & Gardner 1968), one expects the magnetic field direction in the emitting regions to be oriented tangentially. Such a phenomenon is observed in the bilateral SNRs G296.5+10.0 (Milne & Haynes 1994) and G093.3+06.9 (Lalitha *et al.* 1984). A tangential magnetic field need not always be observed, however, since in younger SNRs other factors may cause the magnetic field to be oriented radially (Reynolds & Gilmore 1993; Jun & Norman 1996) or be generally disordered (FR90; Moffett & Reynolds 1994).

One argument against magnetic models is that the typical energy density in the ambient magnetic field is many orders of magnitude less than the kinetic energy of a typical SNR shock (Manchester 1987; Bisnovatyi-Kogan, Lozinskaya, & Silich 1990). However these arguments only pertain to whether the *shape* of a remnant can be influenced by the surrounding field. The brightness distribution can be significantly affected by the ambient field, even if the field is dynamically unimportant (FR90).

6.2. An alternative to the magnetic model

While magnetic models can simply explain bilateral SNRs which have a circular rim and two opposed limbs of similar shape and brightness (e.g. G003.8–00.3 and G327.6+14.6), we now argue that difficulties are encountered when one considers whether such models can also account for the detailed morphologies of other objects in Table 4. As will be discussed in Section 6.2.4, an alternative explanation is the effect of the ISM.

6.2.1. Asymmetric SNRs

There are objects in Table 4 which align closely with the Plane, but for which the flux density and morphology of the bright opposed limbs is very different. The most striking examples of this class are G320.4–01.2 (Figure 8) and G308.8–00.1, but this asymmetry is also present to a lesser extent in G078.2+02.1, G127.1+00.5, G350.0–02.0 (Figure 2) and G356.3–01.5 (Figure 11). In the magnetic model, this morphology can be explained by a gradient in the field strength across the remnant (Caswell & Lerche 1979; Reynolds & Fulbright 1990).

Alternatively, for both G320.4–01.2 and G308.8–00.1, it has been suggested that this appearance is due to the influence of a central pulsar on the surrounding shell (Manchester & Durdin 1983; Kaspi *et al.* 1992; Brazier & Becker 1997), or because one side of the remnant encounters a region of higher density (Seward *et al.* 1983; Kaspi *et al.* 1992). In the latter case, the low value of ψ for these remnants suggests the presence of density gradients perpendicular to the Plane. There is no clear tendency for the limb closest to the Plane to be the brighter of the two. This is contrary to the suggestion of Caswell (1977), although he noted that this may only apply for remnants at large $|z|$.

6.2.2. Distorted SNRs

Some objects are significantly distorted from a circular or elliptical shape, for example G350.0–02.0 (Figure 2) and G166.0+04.3 (Figure 3). Observations of the latter at radio (Landecker *et al.* 1982, 1989), X-ray (Burrows & Guo 1994; Guo & Burrows 1997) and optical (Pineault *et al.* 1985) wavelengths, are all consistent with the model of Pineault *et al.* (1987). As discussed in Section 4.2, this explains the morphology in terms of the shock encountering a hot low density tunnel lying along the Galactic Plane, before propagating into dense material beyond. We have noted that G350.0–02.0 has a similar appearance, which by analogy might also be explained in terms of such a model. The gross morphology of these remnants can be reproduced by magnetic models, but an abrupt change in density by a factor of 100, along an interface parallel to the Galactic Plane, is still required (Mineshige & Shibata 1990).

6.2.3. Elongated SNRs

Some objects in Table 4 are significantly extended along their symmetry axis, most notably G356.3–01.5 (Figure 11) and G296.5+10.0 (Figure 7). This appearance can

be explained by tension associated with the ambient magnetic field, which would cause remnants to preferentially expand along field lines (Insertis & Rees 1991; Mineshige, Shibata, & Shapiro 1993; Różyczka & Tenorio-Tagle 1995). However for typical values of the explosion energy and ambient field strength, the shape of a SNR will not be appreciably distorted by the magnetic field until it reaches a diameter of $\gtrsim$100 pc (Mineshige & Shibata 1990; Norman 1993), at which stage a remnant is nearing the end of its observable lifetime (e.g. Shull, Fesen, & Saken 1989). In order for tension in the magnetic field to account for the observed extension, one must invoke a low explosion energy ($\lesssim 10^{50}$ erg) and/or a high magnetic field ($\gtrsim$ 100 μG). An alternative magnetic explanation for this elongation has been proposed by Roger *et al.* (1988). In the case of G296.5+10.0, they speculate that the SNR shock may not couple to newly swept up material when the magnetic field is parallel to the direction of propagation. As the remnant evolves the shock speed is dependent on the angle with the magnetic field and the remnant will elongate.

Bisnovatyi-Kogan *et al.* (1990) consider a non-magnetic explanation for G296.5+10.0, wherein both the elongation and the bilateral appearance of the SNR are the result of it having expanded into a similarly extended pre-existing cavity. For this mechanism to apply for SNRs with low values of ψ, however, such cavities must lie with their major axis along the Plane.

6.2.4. An ISM model

In the above discussion, we have considered three classes of objects which can be more comfortably accounted for by the surrounding ISM than by the magnetic model. We have considered objects with one side brighter than the other as might be due to a density gradient, a breakout morphology due to the presence of hot tunnels, and elongated remnants which might be due to an extended cavity. In order for any of these explanations to be valid, the observed distribution of ψ requires that structures in the ISM must be consistently parallel to the Plane.

As a mechanism for the bilateral appearance, we propose that the Galactic magnetic field produces density stratifications parallel to the Galactic Plane. Evidence to support this hypothesis is now presented.

The first issue to consider is whether stellar wind-bubbles can be elongated by the surrounding field. Consider a homogeneous ISM of gas density n_H, in which there is a uniform magnetic field of strength B_0. The bubble produced by an isotropic wind will expand more rapidly along field lines than across them, and will begin to be significantly

distorted when the internal pressure in the bubble falls below the external magnetic pressure (Königl 1982). Adapting the result of Stone & Norman (1992) for a wind from a proto-star, this will occur after a time t_1, given by :

$$\left(\frac{t_1}{Myr}\right) \approx 2 \left(\frac{B_0}{3\,\mu\mathrm{G}}\right)^{-5/2} \left(\frac{L_w}{10^{21}\,\mathrm{erg}}\right)^{1/2} \left(\frac{n_H}{\mathrm{cm}^{-3}}\right)^{3/4}, \quad (1)$$

where M is the mass of the star, v_w is the velocity of the wind and $L_w = \frac{1}{2}\dot{M}v_w^2$ is the associated mechanical luminosity. Therefore as a rough criterion, a wind bubble will become significantly elongated along ambient field lines if $t_0 \gg t_1$, where t_0 is the main-sequence lifetime of the star.

Chevalier & Liang (1989) tabulate the properties of stellar wind-bubbles for different spectral types, from which we find that in a typical environment ($B_0 = 3\ \mu$G, $n_H = 1\ \mathrm{cm}^{-3}$), a main-sequence wind-bubble will be dominated by the ambient field for a star of spectral type O9 or later. Such stars comprise the vast majority of the stellar population, and indeed Lozinskaya (1988) notes that wind-blown bubbles are often elongated. Since $t_1 \propto B_0^{-5/2}$, only a slightly higher field than assumed above ($\gtrsim 10\ \mu$G) is required to distort wind-bubbles produced by even the most massive stars. Note that the extra energy input in the late phases of stellar evolution may complicate the simple picture presented here.

On larger scales, Heiles (1979) has found that H I shells within 10° of the Plane appear elongated in the longitudinal direction, which he suggests could also be due to the ambient field. Also, simulations of magnetised superbubbles (Tomisaka 1990, 1992; Mineshige, Shibata, & Shapiro 1993) and old SNRs (Norman 1993) show that such structures also become elongated along field lines, but over larger length and time scales than for stellar wind bubbles.

To summarise, we propose that where the magnetic field is oriented parallel to the Galactic disc, structures will be produced extended in the longitudinal direction, on approximately the same scale as SNRs. Thus close to the Plane, the structure of the Galactic ISM might take the form of tunnels, gradients and cavities all elongated in the disc of the Galaxy. When a SNR interacts with this structure, a bilateral appearance is produced (as in the model proposed by Bisnovatyi-Kogan, Lozinskaya, & Silich 1990), with the axis aligned parallel to the Plane.

A remnant formed from a massive progenitor will interact at its earliest stages with a complex and extensive CSM. During this period, a SNR can take on some aspects of bilaterality (Igumenshchev, Tutokov, & Shustov 1992; Blondin, Lundqvist, & Chevalier 1996; Zhang, Wang, & Chen 1996; Gaensler *et al.* 1997), but no alignment with the

Galactic Plane will be observed (unless the progenitor wind-bubble is elongated along the Plane through the process discussed above). Only once the shock propagates beyond its CSM and begins to interact with the ambient ISM should any trend in ψ manifest itself. Type Ia SNRs such as G327.6+14.6 may interact with the ambient medium at a much earlier stage, however. At the other end of the scale, as a remnant ages and expands, it becomes more and more likely to encounter complex inhomogeneities in the ISM which will distort its appearance. Hence, this mechanism for the bilateral appearance is most relevant for middle-aged remnants, rather than young or old ones. The uncertainty in SNR age estimates prevents us from demonstrating this property in the observed sample. However rough estimates for the ages of SNRs in Table 4 (using the $\Sigma - t$ relation; Caswell & Lerche 1979) give that most are between 1 000 and 10 000 years old.

6.3. Exceptional cases: SNRs G296.5+10.0 and G327.6+14.6

SNRs G296.5+10.0 (Figure 7) and G327.6+14.6 (Figure 9) are discrepant in their values of ψ, both being oriented at almost right angles to the Plane. However, these two remnants are also notable in that they are both at a significant height above the Plane (175–350 pc and 450 pc, respectively; Roger *et al.* 1988).

For bilateral SNRs at low latitudes, we have proposed ISM structures running parallel to the Plane. At higher latitudes, the ISM is dominated by perpendicular structures in the form of chimneys (Norman & Ikeuchi 1989; Normandeau, Taylor, & Dewdney 1996) and "worms" (Heiles 1984; Koo, Heiles, & Reach 1992). Stellar polarization measurements demonstrate the existence of large-scale loops of magnetic field also extending perpendicular to the Plane (Mathewson & Ford 1970). Thus that bilateral SNRs might tend to have $\psi \sim 90^\circ$ at large distances from the Plane is consistent with the extrinsic models described in Sections 6.1 and 6.2.4. SNRs G296.5+10.0 and G327.6+14.6 can therefore still be incorporated within the proposed model. One can speculate that bilateral SNRs at intermediate scale heights might be in transition between remnants with $\psi \sim 0^\circ$ and those for which $\psi \sim 90^\circ$. However the uncertainty in the distances to SNRs in our sample prevents us from making meaningful conclusions on any latitude dependence at present.

These two SNRs are regarded as the prototypes for the bilateral morphology (e.g. KC87; Roger *et al.* 1988). That the most striking examples of bilaterality constitute 50% of known remnants for which $|b| \geq 10^\circ$ may be indicative of the homogeneity of the environment far from the Plane. It is highly likely that the radio all-sky surveys currently being carried out (Large *et al.* 1994; Condon *et al.* 1996) will discover new high latitude SNRs. Whether such remnants also have a well-ordered appearance and a high degree

of symmetry will be useful (but not conclusive) evidence regarding the model we have proposed.

We note that intrinsic models have also been proposed for these two SNRs: Storey *et al.* (1992) argue that the symmetry present in G296.5+10.0 over a wide range of spatial scales generally argues against magnetic models for this object, while Willingale *et al.* (1996) hypothesise that a central compact object with opposed jets could generate the morphology of G327.6+14.6. Whether these remnants represent an extrinsic mechanism operating at high Galactic latitude, or intrinsic effects, either way, their high value of ψ is not at odds with the alignment observed in the remainder of the sample.

6.4. Explanations for non-bilateral structure

As noted in Section 5.2, the vast majority of remnants do not have a clear bilateral appearance. The wide range of SNR morphologies observed (clearly demonstrated in the catalogue of WG96) is indicative that complex, small-scale effects can dominate the appearance of SNRs. Specifically, the absence of bilaterality can be explained by any of the following conditions:

- A dominant component of the field along the line of sight, so that the projection of the emitting region is no longer two distinct arcs of emission. KC87 estimate that a SNR with a cylindrical 3D geometry will appear as a uniform ring of emission with no bilateral appearance if $\theta < 25°$, and will be "confused" if $25° < \theta < 45°$. This results in 24% (rounded to 30% in KC87) of SNRs having a non-bilateral appearance, simply due to orientation.

- An inhomogeneous ISM. In this case, encounters with molecular clouds, cavities, and other inhomogeneities distort a remnant sufficiently so that no symmetrical structure can be observed (e.g. Pineault *et al.* 1993; Reynolds & Moffett 1993; Koo & Moon 1997).

- A disordered ambient magnetic field, so that in the magnetic model, no position angle around the circumference has enhanced emissivity. It is suggestive that some bilaterals are highly polarized (e.g. Lalitha *et al.* 1984; Milne & Haynes 1994), indicating a well-ordered magnetic field.

7. Conclusion

We have presented 1.4 GHz radio observations of two southern supernova remnants, G003.8–00.3 and G350.0–02.0. The morphologies of these two SNRs are distinct — G003.8–00.3 shows a filamentary two-arc appearance in a classic "barrel" shape, while G350.0–02.0 strongly resembles the breakout morphology of G166.0+04.3 (VRO 42.05.01).

Despite their differences, both remnants have a clear bilateral appearance. Furthermore, the axis defined by this classification in both cases aligns almost exactly with the Galactic Plane. On examination of the entire sample of known Galactic SNRs, we find 17 SNRs with a high level of bilateral morphology, of which nine are oriented to the Plane at 12° or less. With a minimum of assumptions regarding the three-dimensional geometry, the probability of this occurring by chance is 7×10^{-4}. Considering SNRs G296.5+10.0 and G327.6+14.6 as distinct from the remainder of the sample reduces this probability even further.

This trend rules out "intrinsic" models for the bilateral morphology, all of which involve an axis defined by the orientation or motion of the progenitor star. Such models are not expected to produce remnants which align in any consistent way with the Galactic Plane.

The general alignment of bilateral remnants with the Plane can be explained by "magnetic" models, whereby an ambient magnetic field generates bright regions around the SNR shell where the shock normal is perpendicular to the field. This is a result of either enhanced field compression or preferential electron acceleration in these regions. However, distorted morphologies in bilateral SNRs can be better explained if the ISM into which these remnants expand consists of structures preferentially elongated in the longitudinal direction. We propose that this occurs in the form of expanding wind-bubbles distorted by the surrounding magnetic field.

The majority of SNRs do not have a distinct bilateral appearance. For some SNRs, this can be explained as an orientation effect, when the bilateral axis is close to the line of sight. The effects of a disordered magnetic field and an inhomogeneous ISM can further account for the observed diversity in morphologies.

This study has demonstrated the value of high resolution observations of Galactic SNRs. Further observations, in particular of the polarization and environment of bilateral SNRs, are needed to test the proposed models. Undoubtedly there also remain more examples of bilateral SNRs to be discovered, particularly in the first quadrant and at high Galactic latitudes, which will improve the available statistics.

While theoretical modelling of the evolution of stellar wind bubbles is quite sophisticated (García-Segura, Langer, & Mac Low 1996 and references therein), the effect of external

magnetic fields is generally ignored. The simple calculations made here suggest that such fields can have a significant effect on the dynamics of a bubble and should be included in subsequent modelling. Similarly, the interaction of SNRs with surrounding material usually assumes spherical symmetry (Chevalier & Liang 1989; Tenorio-Tagle *et al.* 1991); detailed simulations of the interaction of remnants with the (non-spherical) structures proposed here would be highly desirable.

An interesting extension of the results described would be to determine whether bilateral SNRs in other edge-on spiral galaxies are aligned along preferred position angles, and whether these angles correlate with measurements of the corresponding galactic magnetic field. Of particular interest is NGC 4631 which largely has a magnetic field oriented perpendicular to the disc (Hummel, Beck, & Dahlem 1991; Golla & Hummel 1994). At present, existing observations of SNRs in other spiral galaxies (e.g. Duric *et al.* 1993; Muxlow *et al.* 1994) are of insufficient resolution to derive a bilateral subset. However, the planned upgrade to the VLA (Bastian & Bridle 1996) will provide sufficient improvement in sensitivity and resolution to produce images of SNRs in these galaxies of a quality comparable to existing Galactic observations.

I am grateful to Miller Goss and Dale Frail for their help in preparing for the VLA observations, and for their assistance with AIPS and other aspects of data reduction. I also thank Roy Duncan for carrying out the observations made with the Parkes radio telescope, and subsequently reducing and assisting with these data. I would like to thank many people for interesting discussions: John Dickel, John Dickey, Anne Green, Jeff Hester, Tom Landecker, Dick Manchester, Michael Norman, Steve Reynolds, Rob Roger, Brad Wallace and Mark Wardle. David Moffett suggested the possibility that stellar wind-bubbles might be influenced by the ambient magnetic field. Gloria Dubner, Andrew Gray, Anne Green, Tom Landecker and Mike Kesteven kindly provided images of various SNRs. I thank NRAO for hospitality during my visit to Socorro, and acknowledge the financial support of an Australian Postgraduate Award and of the Support for Access to Major Research Facilities programme, administered by the Australian Department of Industry, Science and Tourism. This research has made use of the NASA Astrophysics Data System and of the CDS SIMBAD database.

REFERENCES

Amy, S. W. & Large, M. I. 1990, Proc. Astron. Soc. Austral., 8, 308.

Amy, S. W. & Large, M. I. 1992, Aust. J. Phys., 45, 105.

Bastian, T. S. & Bridle, A. H. 1996, The VLA Development Plan.

Beck, R., Brandenburg, A., Moss, D., Shukurov, A., & Sokoloff, D. 1996, ARA&A, 34, 155.

Becker, R. H. & Helfand, D. J. 1985, Nature, 313, 115.

Berkhuijsen, E. M. 1986, A&A, 166, 257.

Bisnovatyi-Kogan, G. S., Lozinskaya, T. A., & Silich, S. A. 1990, Ap&SS, 166, 277.

Bisnovatyi-Kogan, G. S. & Silich, S. A. 1995, Rev. Mod. Phys., 67, 661.

Blondin, J. M., Lundqvist, P., & Chevalier, R. A. 1996, ApJ, 472, 257.

Bodenheimer, P. & Woosley, S. E. 1983, ApJ, 269, 281.

Brazier, K. T. S. & Becker, W. 1997, MNRAS, 284, 335.

Brighenti, F. & D'Ercole, A. 1994, MNRAS, 270, 65.

Burn, D. & Bush, B. 1994, Private communication.

Burrows, D. N. & Guo, Z. 1994, ApJ, 421, L19.

Caswell, J. L. 1977, Proc. Astron. Soc. Austral., 3, 130.

Caswell, J. L., Kesteven, M. J., Komesaroff, M. M., Haynes, R. F., Milne, D. K., Stewart, R. T., & Wilson, S. G. 1987, MNRAS, 225, 329.

Caswell, J. L., Kesteven, M. J., Stewart, R. T., Milne, D. K., & Haynes, R. H. 1992, ApJ, 399, L151.

Caswell, J. L. & Lerche, I. 1979, MNRAS, 187, 201.

Chevalier, R. A. & Liang, E. P. 1989, ApJ, 344, 332.

Clark, B. G. 1980, A&A, 89, 377.

Clark, D. H., Caswell, J. L., & Green, A. J. 1975, Aust. J. Phys. Astr. Supp., 37, 1.

Condon, J. J., Cotton, W. D., Greisen, E. W., Yin, Q. F., Perley, R. A., Taylor, G. B., & Broderick, J. J. 1996, available on the WWW at http://www.cv.nrao.edu/~jcondon/nvss.html.

Cornwell, T. J., Holdaway, M. A., & Uson, J. M. 1993, A&A, 271, 697.

Cram, L. & Ye, T. 1995, Aust. J. Phys., 48, 113.

Dickel, J. R., Green, A., Ye, T., & Milne, D. K. 1996, AJ, 111, 340.

Dubner, G. M., Giacani, E. B., Goss, W. M., Moffett, D. A., & Holdaway, M. 1996, AJ, 111, 1304.

Dubner, G. M., Giacani, E. B., Goss, W. M., & Winkler, P. F. 1994, AJ, 108, 207.

Duncan, A. R., Stewart, R. T., Haynes, R. F., & Jones, K. L. 1995, MNRAS, 277, 36.

Duric, N., Viallefond, F., Goss, W. M., & van der Hulst, J. M. 1993, A&AS, 99, 217.

Ellis, R. S. & Axon, D. J. 1978, Ap&SS, 54, 425.

Elston, R. & Baum, S. 1987, AJ, 94, 1633.

Falle, S. A. & Garlick, A. R. 1982, MNRAS, 201, 635.

Frail, D. A., Kassim, N. E., & Weiler, K. W. 1994, AJ, 107, 1120.

Frail, D. A. & Kulkarni, S. R. 1991, Nature, 352, 785.

Fulbright, M. S. & Reynolds, S. P. 1990, ApJ, 357, 591 (FR90).

Gaensler, B. M. & Johnston, S. 1995, Publ. Astron. Soc. Austral., 12, 76.

Gaensler, B. M., Manchester, R. N., Staveley-Smith, L., Tzioumis, A. K., Reynolds, J. E., & Kesteven, M. J. 1997, ApJ, 479, 845.

García-Segura, G., Langer, N., & Mac Low, M.-M. 1996, A&A, 316, 133.

Gardner, F. F. & Milne, D. K. 1965, AJ, 70, 754.

Golla, G. & Hummel, E. 1994, A&A, 284, 777.

Gray, A. D. 1994, MNRAS, 270, 847.

Green, A. J. 1972. PhD thesis, University of Sydney.

Green, D. A. 1984, MNRAS, 209, 449.

Green, D. A. 1996, Mullard Radio Astronomy Observatory, Cambridge, United Kingdom (available on the World–Wide–Web at *http://www.mras.cam.ac.uk/surveys/snrs/*).

ed. E. Greisen 1996, The AIPS COOKBOOK, (Charlottesville: National Radio Astronomy Observatory).

Gull, S. F. & Daniell, G. J. 1978, Nature, 272, 686.

Guo, Z. & Burrows, D. N. 1997, ApJ, 480, L51.

Heiles, C. 1979, ApJ, 229, 533.

Heiles, C. 1984, ApJS, 55, 585.

Huang, S.-S. & Struve, O. 1954, Annales d'Astrophysique, 17, 85.

Huang, Y.-L. & Thaddeus, P. 1985, ApJ, 295, L13.

Hummel, E., Beck, R., & Dahlem, M. 1991, A&A, 248, 23.

Igumenshchev, I. V., Tutokov, A. V., & Shustov, B. M. 1992, Soviet Astron., 36, 241.

Insertis, F. M. & Rees, M. J. 1991, MNRAS, 252, 82.

Jokipii, J. R. 1987, ApJ, 313, 842.

Joncas, G., Roger, R. S., & Dewdney, P. E. 1989, A&A, 219, 303.

Jun, B.-I. & Norman, M. L. 1996, ApJ, 472, 245.

Kaspi, V. M., Manchester, R. N., Johnston, S., Lyne, A. G., & D'Amico, N. 1992, ApJ, 399, L155.

Kaspi, V. M., Manchester, R. N., Johnston, S., Lyne, A. G., & D'Amico, N. 1996, AJ, 111, 2028.

Kesteven, M. J. & Caswell, J. L. 1987, A&A, 183, 118 (KC87).

Killeen, N. E. B., Bicknell, G. V., & Ekers, R. D. 1986, ApJ, 302, 306.

Königl, A. 1982, ApJ, 261, 115.

Koo, B.-C., Heiles, C., & Reach, W. T. 1992, ApJ, 390, 108.

Koo, B.-C. & Moon, D.-S. 1997, ApJ, 475, 194.

Lalitha, P., Salter, C. J., Mantovani, F., & Tomasi, P. 1984, A&A, 131, 196.

Landecker, T. L., Pineault, S., Routledge, D., & Vaneldik, J. F. 1982, ApJ, 261, L41.

Landecker, T. L., Pineault, S., Routledge, D., & Vaneldik, J. F. 1989, MNRAS, 237, 277.

Large, M. I., Campbell-Wilson, D., Cram, L. E., Davison, R. G., & Robertson, J. G. 1994, Proc. Astron. Soc. Austral., 11, 44.

Leckband, J. A., Spangler, S. R., & Cairns, I. H. 1989, ApJ, 338, 963.

Lozinskaya, T. A. 1988, in Supernova remnants and the interstellar medium, IAU Colloquium 101, ed. R. S. Roger & T. L. Landecker, (Cambridge: Cambridge University Press), p. 95.

Manchester, R. N. 1974, ApJ, 188, 637.

Manchester, R. N. 1987, A&A, 171, 205.

Manchester, R. N., D'Amico, N., & Tuohy, I. R. 1985, MNRAS, 212, 975.

Manchester, R. N. & Durdin, J. M. 1983, in Supernova remnants and their X-ray emission (IAU Symp. 101), ed. J. Danziger & P. Gorenstein, (Dordrecht: Reidel), p. 421.

Mathewson, D. S. & Ford, V. L. 1970, Mem. R. Astron. Soc., 74, 139.

Milne, D. K. & Haynes, R. F. 1994, MNRAS, 270, 106.

Mineshige, S. & Shibata, K. 1990, ApJ, 355, L47.

Mineshige, S., Shibata, K., & Shapiro, P. R. 1993, ApJ, 409, 663.

Moffett, D. A. & Reynolds, S. P. 1994, ApJ, 425, 668.

Muxlow, T. W. B., Pedlar, A., Wilkinson, P. N., Axon, D. J., Sanders, E. M., & de Bruyn, A. G. 1994, MNRAS, 266, 455.

Napier, P. J., Thompson, A. R., & Ekers, R. D. 1983, Proc. IEEE, 71, 1295.

Norman, C. A. & Ikeuchi, S. 1989, ApJ, 345, 372.

Norman, M. L. 1993, in Back To The Galaxy: AIP Conference Proceedings 278, ed. S. S. Holt & F. Verter, (New York: American Institute of Physics), p. 552.

Normandeau, M., Taylor, A. R., & Dewdney, P. E. 1996, Nature, 380, 687.

Perley, R. A. 1989, in Synthesis Imaging In Radio Astronomy, ed. R. A. Perley, F. R. Schwab, & A. H. Bridle, (San Francisco: ASP Conference Series, Volume 6), p. 259.

Pineault, S. & Chastenay, P. 1990, MNRAS, 246, 169.

Pineault, S., Landecker, T. L., Madore, B., & Gaumont-Guay, S. 1993, AJ, 105, 1060.

Pineault, S., Landecker, T. L., & Routledge, D. 1987, ApJ, 315, 580.

Pineault, S., Pritchet, C. J., Landecker, T. L., Routledge, D., & Vaneldik, J. F. 1985, A&A, 151, 52.

Rand, R. J. & Kulkarni, S. R. 1989, ApJ, 343, 760.

Ratkiewicz, R., Axford, W. I., & McKenzie, J. F. 1994, A&A, 291, 935.

Reich, W., Fürst, E., & Arnal, E. M. 1992, A&A, 256, 214.

Reid, M. J. & Silverstein, E. M. 1990, ApJ, 361, 483.

Reynolds, S. P. & Fulbright, M. S. 1990, Proc. 21st Internat. Cosmic-Ray Conf. (Adelaide), 4, 72.

Reynolds, S. P. & Gilmore, D. M. 1993, AJ, 106, 272.

Reynolds, S. P. & Moffett, D. A. 1993, AJ, 105, 2226.

Roger, R. S. & Costain, C. H. 1976, A&A, 51, 151.

Roger, R. S., Milne, D. K., Kesteven, M. J., Wellington, K. J., & Haynes, R. F. 1988, ApJ, 332, 940.

Różyczka, M. & Tenorio-Tagle, G. 1995, MNRAS, 274, 1157.

Różyczka, M., Tenorio-Tagle, G., Franco, J., & Bodenheimer, P. 1993, MNRAS, 261, 674.

Sault, R. J., Staveley-Smith, L., & Brouw, W. N. 1996, A&AS, 120, 375.

Sault, R. J., Teuben, P. J., & Wright, M. C. H. 1995, in Astronomical Data Analysis Software and Systems IV, ed. R. Shaw, H.E. Payne, & J.J.E. Hayes, ASP Conference Series, Volume 77, p. 433.

Seward, F. D., Harnden Jr., F. R., Murdin, P., & Clark, D. H. 1983, ApJ, 267, 698.

Shaver, P. A. 1969, Observatory, 89, 227.

Shaver, P. A. 1982, A&A, 105, 306.

Shaver, P. A., Salter, C. J., Patnaik, A. R., van Gorkom, J. H., & Hunt, G. C. 1985, Nature, 313, 113.

Shull, J. M., Fesen, R. A., & Saken, J. M. 1989, ApJ, 346, 860.

Slettebak, A. 1949, ApJ, 110, 498.

Sofue, Y. & Fujimoto, M. 1983, ApJ, 265, 722.

Sofue, Y., Fujimoto, M., & Wielebinski, R. 1986, ARA&A, 24, 459.

Stewart, R. T., Caswell, J. L., Haynes, R. F., & Nelson, G. J. 1993, MNRAS, 261, 593.

Stone, J. M. & Norman, M. L. 1992, ApJ, 389, 297.

Storey, M. C., Staveley-Smith, L., Manchester, R. N., & Kesteven, M. J. 1992, A&A, 265, 752.

Tenorio-Tagle, G., Bodenheimer, P., & Yorke, H. W. 1985, A&A, 145, 70.

Tenorio-Tagle, G., Różyczka, M., Franco, J., & Bodenheimer, P. 1991, MNRAS, 251, 318.

Tomisaka, K. 1990, ApJ, 361, L5.

Tomisaka, K. 1992, Proc. Astr. Soc. Jap., 44, 177.

Tuohy, I. R., Clark, D. H., & Burton, W. B. 1982, ApJ, 260, L65.

van der Laan, H. 1962, MNRAS, 124, 179.

Whiteoak, J. B. & Gardner, F. F. 1968, ApJ, 154, 807.

Whiteoak, J. B. Z. & Green, A. J. 1996, A&AS, 118, 329 (WG96).

Williams, R. M., Chu, Y.-H., Dickel, J. R., Beyer, R., Petre, R., Smith, R. C., & Milne, D. K. 1997, ApJ, 480, 618.

Willingale, R., West, R. G., Pye, J. P., & Stewart, G. C. 1996, MNRAS, 278, 749.

Ye, T., Turtle, A. J., & Kennicutt Jr., R. C. 1991, MNRAS, 249, 722.

Zhang, Q.-C., Wang, Z., & Chen, Y. 1996, ApJ, 466, 808.

FIGURE CAPTIONS

Fig. 1.— 1.4 GHz VLA image of SNR G003.8–00.3. The linear greyscale is from –0.5 to 3.0 mJy beam^{-1}, and the peak surface brightness in the image is 15.8 mJy beam^{-1}. The synthesised beam, shown at the lower right of the Figure, corresponds to a resolution of $15'' \times 9''$. The solid line represents a constant Galactic latitude $b = -0.^{\circ}4$. The dashed line represents the axis of symmetry for this SNR, as discussed in the text.

Fig. 2.— Image of SNR G350.0–02.0, produced by combining 1.4 GHz data from the VLA and from Parkes. The linear greyscale is from –2.4 to 7.5 mJy beam^{-1}, and the peak surface brightness in the image is 58.5 mJy beam^{-1}. The synthesised beam, shown at the lower right of the Figure, corresponds to a resolution of $21'' \times 18''$. A line of constant Galactic latitude and the axis of symmetry for the SNR are shown as in Figure 1. Regions A, B and C, as discussed in the text, are indicated.

Fig. 3.— 1.4 GHz image of SNR G166.0+04.3, reproduced from Pineault *et al.* (1987) and precessed to J2000 coordinates. A line of constant Galactic latitude and the axis of symmetry for the SNR are shown as in Figure 1. The "wing" and "shell" components as defined by Landecker *et al.* (1982) are shown.

Fig. 4.— 0.843 GHz image of SNR G315.4–02.3 (RCW 86), reproduced from WG96.

Fig. 5.— 0.843 GHz image of SNR G332.4–00.4 (RCW 103), reproduced from WG96.

Fig. 6.— 1.4 GHz image of G046.8–00.3, reproduced from Dubner *et al.* (1996) and precessed to J2000. Annotations to the image are as in Figure 1.

Fig. 7.— 0.843 GHz image of SNR G296.5+10.0, reproduced from KC87 and precessed to J2000. Annotations to the image are as in Figure 1.

Fig. 8.— 0.843 GHz image of SNR G320.4–01.2, reproduced from WG96. Annotations to the image are as in Figure 1.

Fig. 9.— 0.843 GHz image of SNR G327.6+14.6, reproduced from KC87 and precessed to J2000. Annotations to the image are as in Figure 1.

Fig. 10.— 0.843 GHz image of SNR G332.0+00.2, reproduced from WG96. Annotations to the image are as in Figure 1.

Fig. 11.— 0.843 GHz image of SNR G356.3–01.5, reproduced from Gray (1994). Annotations to the image are as in Figure 1.

Fig. 12.— Histogram of the distribution of ψ, the acute angle between the bilateral axis of a SNR and the Galactic Plane, for SNRs listed in Table 4.

Fig. 13.— Representation of a bilateral SNR in Cartesian space. The vector corresponds to the axis of the remnant, assuming cylindrical symmetry. The observed angle between the projected axis and the Galactic Plane is $\psi = |\phi|$.

Date	Array	Source	Time on source
1996 Jan 20	CnB	G003.7–00.2	$165^{\rm m}$
		G350.0–01.8	$90^{\rm m}$
1996 May 21	DnC	G350.0–01.8	$24^{\rm m}$
1996 Jun 18	DnC	G003.7–00.2	$31^{\rm m}$
		G350.0–01.8	$24^{\rm m}$
1996 Jun 22	DnC	G003.7–00.2	$47^{\rm m}$
		G350.0–01.8	$40^{\rm m}$

Table 1: VLA observations.

Observing date	1996 Sep 07
Centre frequency	1.40 GHz
Bandwidth	40 MHz
System temperature	25 K
RMS noise	24 mJy beam^{-1}
Beam width (FWHM)	$14\farcm85 \pm 0\farcm25$
Map gridding	$6'$

Table 2: Parkes observations.

	G003.8–00.3	G350.0–02.0
VLA pointing centres[1]	$17^{\rm h}55^{\rm m}30^{\rm s}$, $-25^\circ51'00''$	(1) $17^{\rm h}28^{\rm m}30^{\rm s}$, $-38^\circ37'30''$
		(2) $17^{\rm h}27^{\rm m}20^{\rm s}$, $-38^\circ27'30''$
		(3) $17^{\rm h}26^{\rm m}55^{\rm s}$, $-38^\circ10'00''$
		(4) $17^{\rm h}26^{\rm m}00^{\rm s}$, $-38^\circ23'00''$
Resolution	$15'' \times 9''$, PA $= 60^\circ$	$21'' \times 18''$, PA $= -13^\circ$
RMS noise (mJy beam^{-1})	0.06	0.15
Derived centre of SNR[1]	$17^{\rm h}55^{\rm m}28^{\rm s}$, $-25^\circ50'$	$17^{\rm h}27^{\rm m}50^{\rm s}$, $-38^\circ30'$
Derived centre of SNR[2]	003.78, –00.29	349.95, –02.03
Diameter	$13'$	$47' \times 44'$
1.4 GHz flux density (Jy)	1.7 ± 0.1	22.3 ± 0.3
Spectral index	-0.65 ± 0.05	-0.4 ± 0.1
$S_{1\,\rm GHz}$ (Jy)	2.3±0.1	25.7±0.9
$\Sigma_{1\,\rm GHz}$ (10^{-21} W m^{-2} Hz^{-1} sr^{-1})	2.0±0.1	1.7±0.1

Table 3: Observational, measured and derived parameters for each SNR.

[1]Equatorial coordinates α, δ (J2000)

[2]Galactic coordinates l, b

SNR	Other Name	ψ	Figure	Reference
G003.8–00.3		$6° \pm 2°$	1	This paper
G046.8–00.3		$21° \pm 3°$	6	1
G078.2+02.1	γ Cygni	$10° \pm 2°$		2
G093.3+06.9	DA 530	$15° \pm 1°$		3
G127.1+00.5		$3° \pm 3°$		4
G156.2+05.7		$64° \pm 4°$		5
G166.0+04.3	VRO 42.05.01	$2° \pm 2°$	3	6, 7
G296.5+10.0	PKS 1209–51/52	$80° \pm 3°$	7	8, 9
G302.3+00.7		$42° \pm 2°$		10
G308.8–00.1		$9° \pm 3°$		10
G318.2+00.1		$12° \pm 3°$		10
G320.4–01.2	RCW 89, MSH 15–5*2*	$7° \pm 3°$	8	10
G327.6+14.6	SN 1006	$86° \pm 2°$	9	8, 9
G332.0+00.2		$25° \pm 4°$	10	10
G336.7+00.5		$46° \pm 1°$		10
G350.0–02.0		$5° \pm 2°$	2	This paper
G356.3–01.5		$2° \pm 2°$	11	11

Table 4: Bilateral SNRs and their orientation with respect to the Galactic Plane.

References. — (1) Dubner *et al.* (1996) (2) Pineault & Chastenay (1990) (3) Lalitha *et al.* (1984) (4) Joncas, Roger & Dewdney (1989) (5) Reich, Fürst and Arnal (1992) (6) Landecker *et al.* (1982) (7) Pineault, Landecker & Routledge (1987) (8) KC87 (9) Roger *et al.* (1988) (10) WG96 (11) Gray (1994)

This figure "figure1.jpg" is available in "jpg" format from:

http://arXiv.org/ps/astro-ph/9707149v1

This figure "figure2.jpg" is available in "jpg" format from:

http://arXiv.org/ps/astro-ph/9707149v1

This figure "figure3.jpg" is available in "jpg" format from:

http://arXiv.org/ps/astro-ph/9707149v1

This figure "figure4.jpg" is available in "jpg" format from:

http://arXiv.org/ps/astro-ph/9707149v1

This figure "figure5.jpg" is available in "jpg" format from:

http://arXiv.org/ps/astro-ph/9707149v1

This figure "figure6.jpg" is available in "jpg" format from:

http://arXiv.org/ps/astro-ph/9707149v1

This figure "figure7.jpg" is available in "jpg" format from:

http://arXiv.org/ps/astro-ph/9707149v1

This figure "figure8.jpg" is available in "jpg" format from:

http://arXiv.org/ps/astro-ph/9707149v1

This figure "figure9.jpg" is available in "jpg" format from:

http://arXiv.org/ps/astro-ph/9707149v1


This figure "figure10.jpg" is available in "jpg" format from:
http://arXiv.org/ps/astro-ph/9707149v1


This figure "figure11.jpg" is available in "jpg" format from:
http://arXiv.org/ps/astro-ph/9707149v1

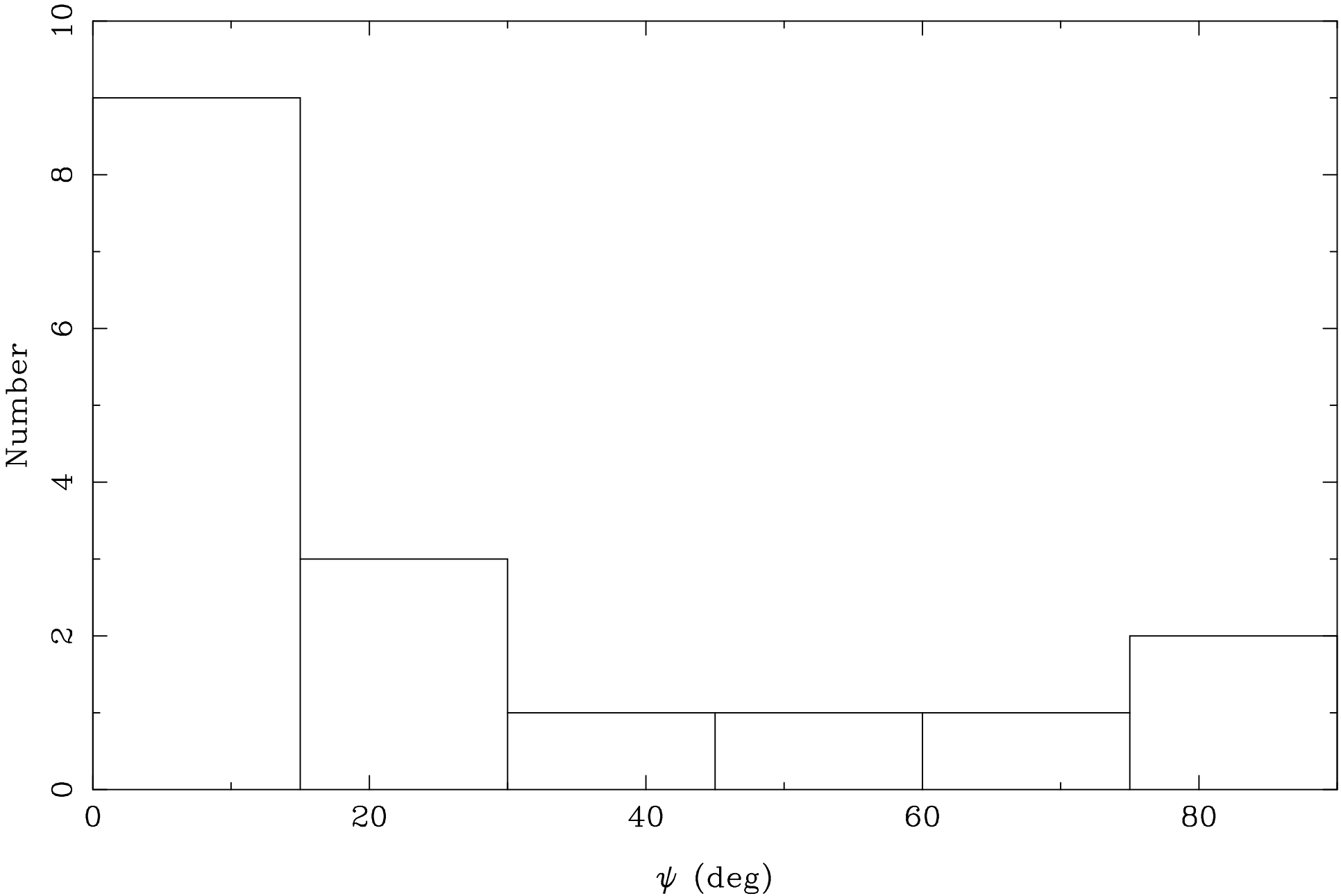
Number
0
2
4
6
8
10
0
20
40
60
80
ψ (deg)

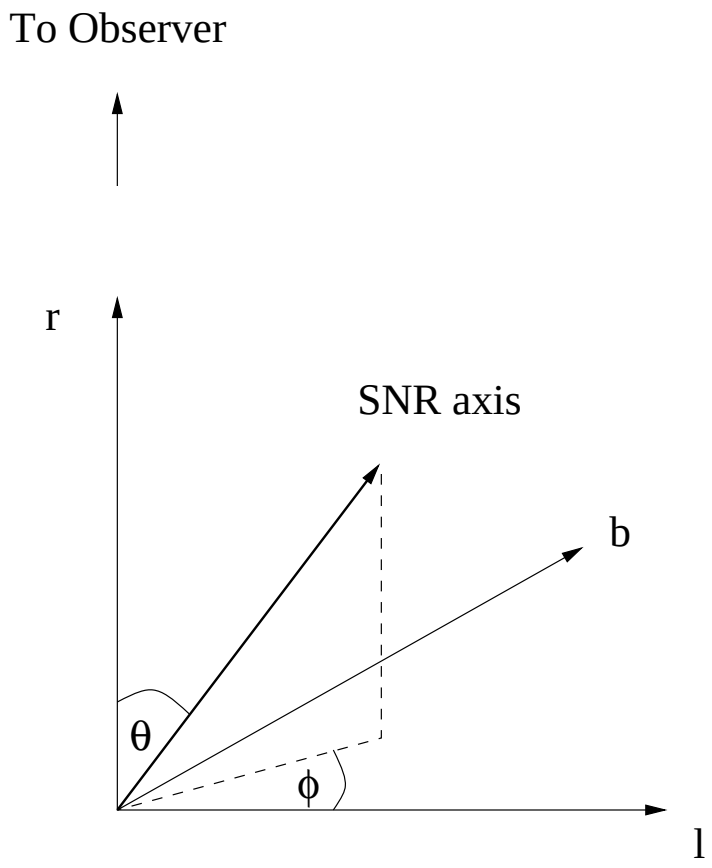
To Observer
r
SNR axis
b
θ
ϕ
l